

Review

Structure, dynamics, and mechanism of the lead-dependent ribozyme

Xin Qi¹ and Tianbing Xia^{2,*}

¹Department of Chemistry, The Scripps Research Institute, Scripps Florida, 130 Scripps Way, Jupiter, FL 33458, USA

²Department of Molecular and Cell Biology, The University of Texas at Dallas, 800 West Campbell Road, Richardson, TX 75080-3021, USA

*Corresponding author
e-mail: tianbing.xia@utdallas.edu

Abstract

Leadzyme is a small catalytic RNA that was identified by *in vitro* selection for Pb²⁺-dependent cleavage from a tRNA library. Leadzyme employs a unique two-step Pb²⁺-specific mechanism to cleave within its active site. NMR and crystal structures of the active site revealed different folding patterns, but neither features the in-line alignment for attack by the 2'-OH nucleophilic group. These experimentally determined structures most likely represent ground states and are catalytically inactive. There are significant dynamics of the active site and the motif samples multiple conformations at the ground states. Various metal ion binding sites have been identified, including one that may be occupied by a catalytic Pb²⁺. Based on functional group analysis, a computational model of the transition state has been proposed. This model features a unique base triple that is consistent with sequence and functional group requirements for catalysis. This structure is likely only populated transiently, but imposing appropriate conformational constraints may significantly stabilize this state thereby promoting catalysis. Other ions may inhibit the cleavage by competing for the Pb²⁺ binding site, or by stabilizing the ground state thereby suppressing its transition to the catalytically active conformation. Some rare earth ions can enhance the reaction via an unknown mechanism. Because of its unique chemistry and dynamic behavior, leadzyme can continue to serve as an excellent model system for teaching us RNA biology and chemistry.

Keywords: conformational constraints; conformational dynamics; leadzyme; metal ion specificity; two-step mechanism.

Introduction

RNAs are ubiquitous products in the cell (1, 2) involved in almost all important aspects of cellular activities (3). RNAs dance around the traditional central dogma as the executors

to render the picture of linear informational flow a four-dimensional affair, in other words, cellular processes are temporally regulated in 3D physical addresses in the cell (4). The discovery of RNAs having enzyme-like catalytic ability, coined ribozyme (5, 6), and the intriguing 'RNA World' hypothesis (4, 7) have stimulated intensive efforts toward the studies of ribozyme structures, dynamics, and mechanisms in the past quarter of a century (8–12).

Ribozymes mostly catalyze phosphoryl transfer reactions (transesterification and hydrolysis); however, if the ribosome is considered, the scope of chemistry is extended to the most important chemical reaction of living matter, namely the peptidyl transfer reaction. These catalytic RNAs have been serving as the modern paradigms for much of what we have learned in RNA biology and chemistry. Atomic resolution structures and folding dynamics of most ribozymes are now available, to go along with extensive biochemical data that provide insights into the detailed mechanics of RNA catalysis (12). Precise structural elements required for catalytic reactions, however, have not been adequately defined for some of these ribozymes, partly due to their rich intrinsic dynamics. This itself is at the forefront of RNA biophysics.

Reviews on ribozymes usually focus on naturally occurring ones, including group I and group II introns, hammerhead and hairpin ribozymes, hepatitis delta virus ribozyme, and ribonuclease P RNA (8–11, 13). More recently, attention has been on the newly discovered ones, including metabolite-sensing riboswitches that also act as ribozymes, e.g., *glms* ribozyme (14–16). A class of ribozyme, namely the lead-dependent ribozyme, or leadzyme, was last reviewed more than 10 years ago (17, 18), and has typically been ignored altogether by review writers since. The authors of this review speculate that this was perhaps in part due to its artificial nature and seemingly limited scope as a model system. Leadzyme, however, has some unique features compared to other ribozymes, and it has its special place in RNA biology (17). It can be argued that an RNA catalyst as simple as the leadzyme can still be an excellent model system for learning new RNA biology and chemistry and can continue to serve as a learning tool. This review summarizes research on this system during its own quarter of a century development, including more recent exciting work using state-of-the-art biochemical and biophysical approaches that have yet been employed on those natural ribozymes.

Origin of the leadzyme motif

The first 'artificial' ribozyme discovered was believed to be yeast tRNA^{phe}, which cleaves itself between D17 and G18

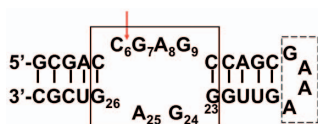


Figure 1 Secondary structure of the leadzyme. The box region is the active site, and the red arrow indicates the scissile bond. The GAAA tetraloop in the dashed box is sometimes used to render the construct unimolecular.

in the D-loop into two fragments of well-defined lengths in the presence of lead ions (Pb^{2+}) (19–22), therefore it has its historical place in the field of chemistry of RNA catalysis (23). The cleavage reaction seemed to depend more on the conformation than the sequence, with bends in the tRNA tertiary structure being more sensitive to Pb^{2+} -dependent cleavage, making the reaction a useful probing method for tRNA structures (21, 22). This served as a good model for RNA catalysis because of the availability of the high-resolution structures of both the uncleaved and cleaved states (20). Discovery of tRNA^{phe} autocleavage in the presence of Pb^{2+} led Uhlenbeck and coworkers to use an *in vitro* selection method on libraries of tRNA^{phe} to isolate RNA molecules that also undergo self-cleavage with Pb^{2+} faster than the tRNAs (24). After six rounds of selection using a circular intermediate, they defined a small lead-dependent self-cleaving RNA motif, coined the leadzyme motif (25). Although derived from yeast tRNA^{phe} fragments, the leadzyme motif did not fold like any elements of tRNA. In the leadzyme motif, the cleavage site is located within an asymmetric four-by-two purine-rich internal loop (Figure 1) flanked by helices on both sides (25, 26). In the presence of Pb^{2+} , the leadzyme motif undergoes autocleavage of the phosphodiester bond between C6 and G7 in the longer strand. Subsequent structural and mechanistic studies often employed leadzyme constructs either as a unimolecular hairpin design capped by a stable GAAA tetraloop (25–30) or in a two-piece duplex form (25, 31–38).

Lead ion-dependent cleavage activities have also been found in other RNAs, e.g., the D-loop of 5S rRNA (39) and RNase P RNAs (40). In fact, the leadzyme motif and its close variants have been found to be common in eukaryotic genomes and have since been implicated in lead toxicity *in vivo* leading to many human disorders including cancer (20, 41). Recently, it has been shown that lead-dependent site-specific RNA cleavage can be used to inhibit tobacco mosaic virus infection (42). The potential therapeutic value of leadzyme motifs is promising but needs to be further explored.

Unique Pb^{2+} -specific two-step cleavage mechanism and kinetics

RNA-metal ion interactions have been one of the focuses of RNA folding, thermodynamics (43–45) and function, particularly catalysis of ribozymes (46–50). In the tRNA^{phe}, the cleavage involves removal of the proton from the 2'-OH of ribose-17 by a Pb^{2+} -bound hydroxyl group above pH 7 (20),

and this was facilitated by pKa of the Pb^{2+} -bound water molecule being close to 7 making it an effective RNA cleavage agent (51). Nucleophilic attack of the resulting 2'-O⁻ on the adjacent phosphate-18 produces the chain scission. A penta-coordinate phosphorus cyclic intermediate is presumably involved.

The leadzyme is a rich source for learning RNA metal-loenzymology (17). The leadzyme cleavage is highly specific for Pb^{2+} ion (26). The cleavage reaction rate is exponentially dependent on pH between 5.5 and 7.0 (26) as was observed in the lead-induced cleavage of tRNAs (20), suggesting hydroxide groups coordinated to Pb^{2+} also act as a general base in the rate-limiting step of the cleavage reaction (26), where it abstracts a proton from the nucleophilic 2'-OH of C6. At high concentration of Pb^{2+} or at high pH values, polyhydroxides or polyhydrates form (51) that cannot bind the active site of leadzyme, therefore resulting in reduced cleavage (26). At least 25 other divalent or trivalent cations are not able to induce specific cleavage within the leadzyme motif alone but some, particularly rare earth ions (Nd^{3+} being the best), can enhance the cleavage reaction (31, 32).

Similar to tRNA cleavage, Pb^{2+} ion initiates cleavage within the leadzyme motif via attack by the 2'-OH nucleophile of the C6 sugar on the phosphate group, forming the 2',3'-cyclic phosphate and the 5'-OH products (Figure 2A) (25). This step is similar to other ribozyme cleavage reactions in hammerhead, hairpin, and hepatitis delta virus ribozymes, where the 2',3'-cyclic phosphate is the end product (12). The leadzyme cleavage reaction, however, is unique among known ribozymes in that it undergoes a two-step mechanism (Figure 2A), in which the intermediate product 2',3'-cyclic phosphate group formed from the first step is specifically hydrolyzed to generate the 3'-mono phosphate as the end product, a step that is also Pb^{2+} -dependent (25, 30) and similar in mechanism to strand cleavage by RNase A.

Although the 2',3'-cyclic phosphate intermediate cannot be easily resolved by traditional gel electrophoresis-based techniques, its presence was initially observed by thin layer chromatography (25). Recently, a high-resolution ion-exchange HPLC-based assay for monitoring the full kinetic progress of leadzyme self-cleavage was also developed to resolve the 2',3'-cyclic phosphate product from the first step and the 3'-mono phosphate product from the second step in the early time traces (Figure 2B), as well as to monitor the conversion from the former to the latter (30). The wild type leadzyme cleaves with an overall kinetic rate constant of $\sim 1.4 \text{ min}^{-1}$ ($\tau \sim 0.7 \text{ min}$) at $200 \mu\text{M}$ Pb^{2+} , consistent with earlier reports under similar conditions (25, 26, 29, 33, 38). The kinetics of two-step cleavage reaction can be described by the following four equations:

$$P_{30mer}(t) = e^{-t/\tau} \quad (1)$$

$$P_{24mer}(t) = 1 - e^{-t/\tau} \quad (2)$$

$$P_{6mer(2,3'\text{-cycP})}(t) = (1 - e^{-t/\tau})e^{-t/\tau} \quad (3)$$

$$P_{6mer(3'\text{-P})}(t) = (1 - e^{-t/\tau})(1 - e^{-t/\tau}) \quad (4)$$

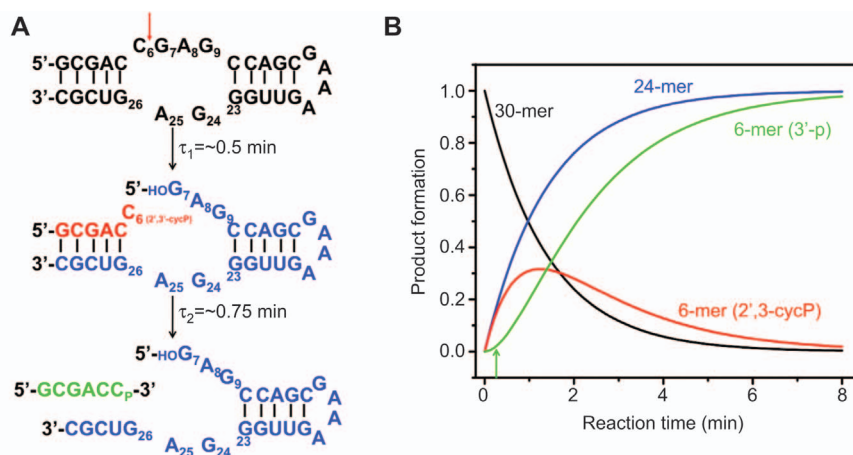


Figure 2 Cleavage reaction of leadzyme and kinetics.

(A) The two-step cleavage reaction. The red arrow indicates the scissile bond. The first step cleaves the parental 30-mer hairpin (black) to generate the 24-mer hairpin with 5'-OH group (blue) and the 6-mer with 2',3'-cyclic phosphate group (red). The second step hydrolyzes the 2',3'-cyclic phosphate group to generate the 6-mer with 3'-monophosphate (green). The lifetimes of the two steps are ~ 0.5 min and ~ 0.75 min, respectively in $300 \mu\text{M Pb}^{3+}$. (B) Kinetic profiles of the cleavage reaction. Curves are color-coded to match those in (A). The green arrow points to the lagged appearance of the 6-mer (3'-P).

where P represents products and τ_1 and τ_2 represent the lifetimes of the first and second reactions (or inverse of rate constants). The decay of the parental 30-mer and the appearance of the 24-mer product only depend on the first step and they follow the same overall kinetics ($\tau \sim 0.7$ min). Note the individual kinetic rates of initial build-up ($\tau_1 \sim 0.5$ min) and the subsequent decay of the 2',3'-cyclic phosphate 6-mer product that led to the lagged appearance of the final 3'-mono phosphate 6-mer product ($\tau_2 \sim 0.75$ min). Such conversion between the two 6-mer products can be inhibited by addition of EDTA at the peak of the build-up of 2',3'-cycP 6-mer product (30), suggesting that the second step of the reaction also requires the presence of Pb^{2+} ion as well as the structural context of properly hybridized initial cleavage reaction products of 6-mer and 24-mer (25, 36, 52). The two steps have very similar catalytic rate constants.

High-resolution structural models

A number of high-resolution structures of ribozymes have appeared in the past decades, and they provide opportunities for understanding structure-function relationships for these functional RNAs (12). However, sometimes the structures alone could not completely account for the findings by extensive biochemical probing. Currently, the precise chemistry underlying RNA catalysis is a hotly pursued research area.

Leadzyme is one of the smallest catalytic RNA domains, but its surprising complexity in the reaction mechanism compared to those naturally occurring larger ribozymes makes it an attractive model system for understanding the structural and thermodynamic basis of RNA catalysis (18) using a battery of structural biology tools, including NMR (27, 28, 35, 53–56), circular dichroism spectroscopy (30, 34, 35, 57),

X-ray crystallography (36, 37), ultrafast time-resolved fluorescence spectroscopy (30), and molecular modeling (18, 33, 52). Interestingly, these structural studies produced multiple models that are distinct in subtle but important ways in the precise conformations of the active loop region (Figure 3).

In fact, the NMR solution structure of the leadzyme determined in the Pardi laboratory represents the first structure of a ribozyme determined in its entirety (17, 27, 55). The solution structure was determined in the absence of Pb^{2+} at pH 5.5, and suggested the formation of a protonated $\text{AH}^+25\text{-C6}$ wobble base pair with two hydrogen bonds next to the cleavage site (Figure 3A). The pK_a of N1 of A25 was determined to be only 6.5 (54, 56), much higher than its typical value of ~ 3 , to facilitate the formation of the protonated wobble pair with C6 at the experimental pH value. The protonation/deprotonation chemical exchange occurs on a $\sim 30\text{--}47 \mu\text{s}$ timescale (56, 58). Such a protonated $\text{AH}^+\text{-C}$ wobble base pair has been observed in loop A of the hairpin ribozyme, also next to the cleavage site (59). At neutral pH, a stable CA pair was not observed in the leadzyme (35). Replacing this wobble pair by an isosteric GU wobble abolishes the activity (28). The bases of the asymmetric internal loop are mostly folded in with the A8 and G24 forming a sheared pair, but neither is well defined and G24 is flipped out $\sim 20\%$ of the time. G7 and G9 are flipped out. The pattern of protection in chemical probing experiments is consistent with the folded structure in solution. Notably, however, the scissile phosphate between C6 and G7 is not aligned for the in-line attack by the 2'-OH of C6. Therefore, apparently the leadzyme motif must undergo some conformational change, at least locally, to reach the catalytically active conformation, reminiscent of what has been observed in the hammerhead ribozyme (60–63).

No significant structural changes were observed upon addition of monovalent Na^+ or divalent Pb^{2+} and Mg^{2+} ions

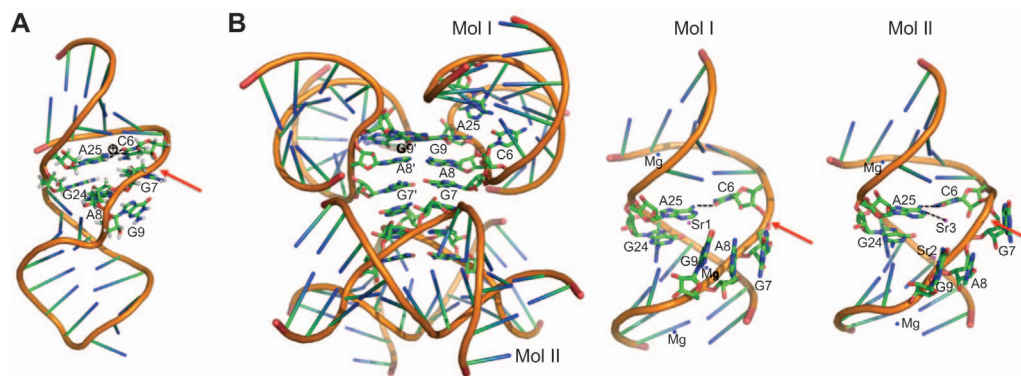


Figure 3 High-resolution structural models of leadzyme.

(A) NMR solution structure of leadzyme. Only the active site residues are shown as stick models. The protonated base pair A25H⁺-C6 is indicated. (B) Crystal structures of leadzyme showing (left) crystal packing among the four molecules in asymmetric unit; (middle) Mol I; and (right) Mol II. Metal ions are shown as small spheres. Red arrows indicate the scissile bond.

(28), suggesting that the tight metal ion binding sites are preformed in the absence of divalent ions. Effects of Pb²⁺ on the solution structure were also analyzed by NMR in the Uesugi group using leadzyme constructs with the 2'-OME group incorporated at C6 to prevent cleavage (35). Changes in the imino proton chemical shift upon Pb²⁺ addition were used to probe the possible Pb²⁺ binding sites. Overall, two metal binding sites were identified; one involves G26, suggesting a possible Pb²⁺ binding site that is close to the cleavage site. Involvement in Pb²⁺ binding by N7 of G26 was also implicated based on effects of functional group substitution on the cleavage reaction (30). The second is composed of G7 and A8. In addition, Mg²⁺ and Pb²⁺ compete for these sites. Such solution probing of metal ion binding sites is echoed by X-ray crystallography discussed later in this review.

The crystallographic studies by Wedekind and McKay in the presence of Mg²⁺, Ba²⁺, and Pb²⁺ ions produced two independent structures within the asymmetrical unit at a modest 2.7 Å resolution (36) and were later refined to have four molecules per asymmetric unit in the presence of Mg²⁺ and Sr³⁺ ions with higher resolution (1.8 Å) to compare to Mg²⁺-only condition (37). The two types of structures are similar in overall fold (RMSD ~ 1.9 Å between the two crystal structures) but have distinct features in the details within the active site (Figure 3B), and both structures are also different from the NMR structure (RMSD ~ 5.3–5.6 Å between NMR and crystal structures) mainly in whether A25 and C6 form a protonated A⁺-C pair, and how the purine bases are arranged within the internal loop (17). In both the crystal structures, there is only one single hydrogen bond between the O2 group of C6 and the amino group at N6 of A25, and A25 is not protonated. The two bases on the shorter strand G24 and A25 are in stacking continuity with the helical regions; the three residues G7, A8 and G9 on the longer strand that are 3'- to the cleavage site, however, are all flipped out. Therefore, there is no shear base pair between A8 and G24 as observed in the NMR solution structure (Figure 3A).

The two structures in the crystal lattice have some interesting differences (Figure 3B). In one structure (Mol I), the three purine bases G7-A8-G9 form a continuous stacked triple almost perpendicular to the helical axis; in the other structure (Mol II), only A8 and G9 are stacked, and G7 is unstacked from A8 thus creating a sharp kink in the backbone at the scissile bond, which is a distinct feature from Mol I. In addition, C6 adopts a C2'-endo sugar pucker in Mol II compared to the regular C3'-endo in Mol I. Neither of the two crystal structures has the scissile phosphate group precisely aligned for the in-line attack, but Mol II was hypothesized to be closer to the transition state or pre-catalytic state because it only needs to undergo limited conformational rearrangement to reach the transition state (36, 37). Mol I was considered ground state. It should be noted that these flipped out bases are apparently involved in extensive crystal contacts, featuring inter-molecular purine-purine hydrogen bonds involving both the Watson-Crick and Hoogsteen faces and vertical base-base stacking interactions, thereby forming parallel helices of hexanucleotide stacks (23). Therefore, the precise geometry of the active site observed in these crystal structures is likely significantly influenced by these intermolecular interactions that are not operating in an isolated leadzyme molecule in solution. As is discussed below, ultrafast dynamics probing suggested that such a stacked triple does not exist in detectable population in solution (30). One must therefore be cautious in drawing the relevance of the observed structures to catalytic mechanism.

More significant is that the crystal structures provided a detailed picture of various binding sites for metal ions, including Mg²⁺, Ba²⁺, Pb²⁺, and Sr³⁺. Sr³⁺ ion has an ionic radius (1.13 Å) similar to that of Pb²⁺ (1.12 Å) and therefore can mimic Pb²⁺. Most of the observed metal ion binding sites are localized in the deep groove of the motif close to the Hoogsteen region (23) but they are different in terms of number of ions bound and precise locations between Mol I and Mol II. Mol I binds two Mg²⁺ ions and one Ba²⁺ ion (36) or three Mg²⁺ (37). The first Mg²⁺ is bound to O6 of G3

and the second bound to O6 of G23, also close to A8 and G9, similar to the positions identified by NMR (35). These two positions are also found in Mol II. A third Mg^{2+} site was only found in the ground state Mol I binding to G22 and G23. The Ba^{2+} ion is bound to O6 of G26, also similar to that identified by NMR (35). Mutation of G26 to 7-deazaguanine where the N7 is changed to CH significantly decreases leadzyme activity, suggesting that N7 of G26 may also be involved in metal binding (30). When Sr^{3+} is soaked together with Mg^{2+} , Sr^{3+} was observed to bind to additional sites (Figure 3B). One Sr^{3+} ion (Sr1) binds in the ground state Mol I contacting G23, G24 and A25 (37).

Mol II binds two Ba^{2+} strongly and one weakly (36). The minor Ba^{2+} site is close to O6 of G26, similar to that in Mol I. One of the major Ba^{2+} sites is near G22 and can be alternatively occupied by Mg^{2+} and Pb^{2+} , similar to a Mg^{2+} site in Mol I, suggesting this is a dominant site for metal ion binding with a structural role (36). For the other major site, the Ba^{2+} is bound to the N1 of A25 and is close to the 2'-OH of C6 and the scissile bond. In the presence of Sr^{3+} , there are two Sr^{3+} sites (Sr2 and Sr3) (37). Sr2 occupies one of the Mg^{2+} sites in Mol I; Sr^{3+} binds near the scissile bond, interacting directly with N1 of A25 and is also close to the 2'-OH of C6, similar to one of the Ba^{2+} sites observed earlier. This site was hypothesized to mimic the binding of the catalytic Pb^{2+} ion to activate the 2'-OH of C6. However, this does not easily explain why A25 can be replaced by a number of other residues or even be an abasic site without affecting cleavage activities (33).

In the crystal lattice, the leadzyme is active, and site-specific cleavage can occur, albeit with an order of magnitude slower rate. Extended exposure to Pb^{2+} disorders the crystals preventing direct probing of Pb^{2+} sites. The Mol I in the crystal lattice is unlikely to be able to undergo the substantial conformational changes needed for the catalytically competent form. The Mol II is much closer to the catalytic conformation. Abstraction of the 2'-OH ribose proton may be followed by a sugar pucker change from C2'-endo to C3'-endo and together with slight twisting of the phosphodiester bond that allows the attacking nucleophile to be in-line with the 5'-phosphate leaving group on G7. This led the authors to propose that this represents the pre-catalytic conformation that transitions from that in Mol I which is the 'non-catalytic' ground state. The fact that Mg^{2+} prefers Mol I over Mol II suggested that Mg^{2+} can act as a competitive inhibitor (26) by favoring non-catalytic conformations (36, 37).

It has been observed that certain rare earth ions (e.g., Nd^{3+}) can enhance the cleavage yield (31) and the rate constant is maximal when Pb^{2+} and Nd^{3+} are at 1:1 ratio (32). This led to a two-metal binding site mechanistic proposal, where both Pb^{2+} and Nd^{3+} directly participate in the activation, playing the role of general base and general acid catalyst, respectively, where Pb^{2+} abstracts the proton from the 2'-OH and Nd^{3+} coordinates with the leaving 5'-oxygen (32). The observations based on the metal ion binding sites in the crystal structures, however, disputed the direct role of two metal ions, where a single Pb^{2+} ion participates in the catalytic mechanism (37). This should be considered an unresolved issue for further research.

Sequence and functional group requirements for cleavage

Mutational studies are at the core of enzyme mechanism analysis. Effects of mutations for all the internal loop residues of leadzyme on its activity were analyzed using *in vitro* selection (26), residue deletion (57), and functional group substitutions (30, 33), providing a detailed picture of the sequence and functional group requirements for cleavage.

The position at 6 highly prefers C (26, 33), and cannot be U presumably to prevent formation of a Watson-Crick base pair with A25; and neither adenine nor guanine was selected for this position. Most purine bases or purine analogs, guanine, adenine, inosine, 2-aminopurine, 7-deazaadenine, and 7-deazaguanine (except for 2'-deoxy 7-deazaguanine) can be tolerated at position 7 (30, 33), but C is never found at this position (26) so that it will not form a stable base pair with G24. For position 8, neither pyrimidine bases U or C were found during the selection (26), but it can tolerate adenine and guanine. Other purines at this position, e.g., 2-aminopurine or 7-deazaadenine, however, decrease the activity 30-fold and 2–7-fold, respectively (30, 33). Both positions 9 and 24 strongly prefer a guanine base (26), and all other purine analogs at least partially reduce the activity (30, 33). Position 25 is the most variable one. It can be replaced by a variety of natural bases or base analogs or even as an abasic site without significantly affecting the cleavage, and some even lead to enhancement (30, 33). The only exception is guanine because it would likely form a Watson-Crick base pair with C6.

In addition, the 2'-OH and N7 groups of G26 in the stem seem to be important (30, 33). Presumably they are involved in metal ion binding (30). Inversion of C5-G26 base pair to G5-C26 pair leads to 20-fold reduction in activity (33).

Molecular modeling of the catalytic transition state by MC-SYM

Taking together the mutational studies, the three nucleotides, C6, G9, and G24, were found mostly invariant, at the functional group levels, in order for the leadzyme motif to remain active (26, 33). This provided important clues on the catalytically relevant conformations of leadzyme because all the active variants have to mimic the same conformations along the reaction pathway. These functional group modification data allowed Cedergren, Major and coworkers to apply the principle of the intersection of conformational space (ICS) to model the active conformations common to leadzyme and its active analogues from initial models generated using MC-SYM and refinement by molecular mechanics energy minimization (18, 33, 52). The resulting model (Figure 4A) that is consistent with all known modification data features a hydrogen-bonded base triple formed by C6, G9, and G24, in which C6 and G24 form a reverse Watson-Crick pair, and G9 pairs with G24 in an asymmetric way (Figure 4B) (64). G7 is flipped out but A8 stacks on G9. The C5-G26 pair is a reverse Watson-Crick pair, with G26 in *syn* conformation. A25 is not required for cleavage, suggesting that this base is

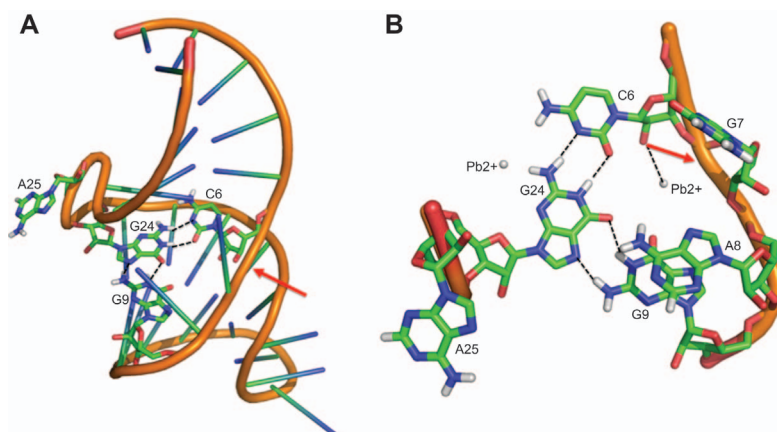


Figure 4 MC-SYM model of leadzyme that is relevant to catalysis.

(A) Full structural model. Only C6, G9, and G24 forming the base triple and A25 are shown as stick models. Hydrogen bonds in the base triple are indicated by dashed lines. The red arrow points to the scissile bond. (B) Close view of the base triple and the bulged out A25. Red arrows indicate the in-line attack by the 2'-OH of C6 on the adjacent phosphate. Locations of two Pb^{2+} ions are represented by gray spheres.

bulged out in the transition state, different from all of the high-resolution structures. This argues against the potential functional role of the high pK_a of 6.5 for N1 of A25 in the cleavage reaction (27, 54, 56), and is consistent with the variable nature of this position. However, lack of specific interactions for a base in the transition state does not necessarily mean it will not affect functions. For example, replacing A25 by 2-aminopurine, 6-methyl U, or an abasic site can enhance leadzyme activity (30, 33), presumably due to their tendency to flip out and allow the formation of base triple; while replacing A25-C6 pair with an isosteric G-U wobble pair eliminates activity (28) because of the higher barrier for flipping out base 25 (58). Such a phenomenon has also been observed in RNA aptamer-ligand recognition, where a base that is bulged out in the ligand-bound complex of the theophylline aptamer can play an important role during the recognition because its interactions involved in the free RNA state (65, 66).

The computational model has a significantly different backbone conformation at the active site compared to the NMR and crystal structures. One of the main differences in these structural models concerns the orientation of the G bases in the active sites, and there is one single but different G that adopts *syn* conformation in these structures. In the computational model, the G24 in the base triple is in *syn* conformation (52). This differs from crystal structures in which G9 is in *syn* conformation in three of four structures, and in *anti* conformation in the other structure (37). In NMR structure, the G7 is in *syn* conformation, G9 and G24 are in *anti* and G24 is engaged in base stacking interactions with A25 (27). The G9 and G24 positions are essential for catalysis while the identity of G7 is not (25, 26, 33), and conformational changes between *syn* and *anti* forms of relevant guanine bases necessarily lead to disruption of their respective structures. Therefore, only one of the three structural models can be the catalytically relevant active conformation of leadzyme. Because it is the MC-SYM model, not the

NMR solution structure or X-ray crystal structures, that satisfies all the sequence and functional group requirements of an active leadzyme, and the 2'-OH of C6 is aligned with the leaving group of 5'-phosphate of G7 ready for in-line attack, the base triple model most likely represents the transition state of cleavage reaction. Such a structure, however, can only exist with very low population or transiently, escaping detection by NMR. The NMR structure is the average ground state, while the crystal structure is biased by the crystal contact involving G7-A8-G9. The conversion from the ground state to the transition state dictates the slow catalytic rate of ribozymes.

In light of this base triple model, functional groups that are important for Pb^{2+} binding were analyzed and the model predicted two Pb^{2+} binding sites (Figure 4B) (52). One Pb^{2+} can potentially be bound by the base triple and positioned close to the cleavage site to interact with C6 to promote nucleophilic attack. This site is similar to those identified by high-resolution structural analyses. A second Pb^{2+} may bind to G24 and the reverse Watson-Crick C5-G26 base pair, explaining the loss of activity by 7-deazaguanine at position 26 (30) and switching C5-G26 to G5-C26 pair (33).

Effects of conformational constraints on cleavage activities

The small size of leadzyme also renders it an excellent system for employing modern synthetic chemistry strategies to test whether manipulations on local conformational constraints impact RNA functions. Two recent exciting studies looked into whether locking either the base or sugar in a particular conformation site-specifically may favor or inhibit catalysis (29, 38).

The Bevilacqua laboratory constructed leadzymes with 8-bromoguanine (8BrG) incorporated at the three guanine positions, G7, G9, and G24, in the active site individually to

analyze the catalytic relevance of different structural models which feature different guanine bases in *syn* conformation (38). The conformationally restricted 8BrG strongly favors a *syn* conformation due to its bulky substitution at C8 position of the modified base. Kinetic assays on these modified leadzyme constructs showed that 8BrG at position 24 renders the leadzyme hyperactive, leading to as much as a 30-fold increase in cleavage rate, compared to reduced activities for leadzyme constructs with the 8BrG modifications at G7 or G9 positions, which slowed down the cleavage reaction by 3- and 23-fold, respectively. These findings lent direct support for the computational model of the leadzyme, where G24 is in *syn* conformation, as the most relevant conformation to the phosphodiester bond cleavage. Presumably each guanine base may exist as an equilibrium between *anti* and *syn* conformations, and depending on the location, render the leadzyme active or inactive. The overall catalytic rate depends on a productive sampling of appropriate glycosidic torsion angle by each G base collectively. Apparently, the modified base 8BrG at G24 pre-organizes the active site into a catalytic competent conformation that requires a *syn* glycosidic torsion angle at this position, to form the base triple with C6 and G9 as proposed by the computational model (Figure 4B). The NMR and crystal structures with G24 in *anti* conformation represent ground states and have to undergo significant conformational rearrangements, at least involving the rotation of G24 glycosidic bond to reach the catalytically active form (38).

In a separate report, the Hoogstraten laboratory used locked nucleic acids (LNA) as a functional probe to address the conformational constraints in leadzyme (29). LNA restricts the ribose to C3'-endo sugar pucker, which allows one to assess the impact of ribose structure and dynamics on the function. The three guanine bases, G7, G9, and G24, were also selected for this analysis. LNA at G7 slightly reduced the reaction rate (~ 2 -fold), consistent with the previous findings that this position can tolerate a number of different residues (26, 30, 33). More reduction in rate was observed by LNA at G24 (~ 15 -fold) suggesting that the modification suppressed the transition from the ground state with C3'-endo to catalytic state featuring a C2'-endo pucker (52). Note that the 8BrG substitution at G24 that enhanced the cleavage would favor a C2'-endo pucker at this position (38). By contrast, LNA at G9 produced the most dramatic increase in the rate by more than 20-fold. G9 adopts C2'-endo pucker seen in the NMR and crystal structures, but C3'-endo in the MC-SYM model (52). The rate enhancement by LNA at G9 is again consistent with the MC-SYM model representing the catalytic active state, and is consistent with the fact that conformational changes are key events for catalysis.

These studies showed that by introducing conformational constraints, conformational equilibrium can be shifted to favor the set of preferred torsion angles that collectively define the catalytic transition state. Such a transition state can be modeled by functional group analysis but is otherwise only populated transiently or with low abundance without the conformational constraints. Therefore, the apparent disconnection between high-resolution structural models and bio-

chemical probing can be reconciled by modeling of the transition state with high resolution. Such modeling efforts need to be experimentally validated by approaches discussed here, and other ingenious approaches for imposing conformational bias can provide more insights. It remains to be seen whether the different perturbations on the base and ribose moieties produce additive effects if applied simultaneously (29). Limited studies suggested that this is likely (30).

Conformational dynamics of the active site of leadzyme motif

The above discussions underpin the important role of RNA conformational dynamics. RNA can notoriously adopt multiple conformations, the so-called conformer hell problem (67). RNA folding and function should be considered as four-dimensional problems (68), in which both spatial coordinates (structure) and their time-dependent behavior (dynamics) are essential information. The ability of RNAs to undergo conformational dynamics is often a prerequisite for their functional repertoire (69). The dynamic behaviors of RNA structures necessarily imply structural heterogeneity at a given moment depending on the exact timescale being considered. Therefore, the conformational dynamics and the resulting heterogeneity are part of the picture of the structure-dynamics-function relationship (70).

The fact that there are multiple structures that have been captured or proposed by different techniques suggests that the leadzyme is structurally dynamic. It is most likely that all the experimentally observed structures (Figure 3) represent a few from an ensemble of conformations that can be adopted by the leadzyme motif at ground state under a given condition and that they interconvert over certain timescales. The catalytically active form (Figure 4) is not populated significantly. Therefore, a certain degree of conformational rearrangement is necessary for the proposed in-line nucleophilic attack on the scissile phosphodiester bond.

NMR studies on leadzyme provided the first direct evidence of conformational dynamics at the active site in the RNA structure-dynamics-function relationship (17, 27, 28, 55, 56, 58). NMR ^{13}C relaxation experiments revealed rich molecular dynamics at the active site that occur on various timescales. The helical regions appeared to be quite rigid (28). Rigidity of base 25 when protonated is comparable to that of the helical region, but it undergoes exchange between the protonated and deprotonated states on a 30–47 μs timescale (56, 58), with a population distribution of 10:1 between protonated and unprotonated states (27). The MC-SYM model, however, suggests that this base has to bulge out for catalysis (33, 52). Un-pairing of A25 from C6 is necessary for transitioning to the active conformation (27, 28, 58), which allows C6 to form base triple with G9 and G24 (33, 38). The phenomenon of opening of alternative base pairs in the free RNA in the ground state for ligand recognition or proper folding has also been observed in other RNA systems, e.g., theophylline aptamer (65, 66) and purine riboswitch RNAs (71–73).

A8, however, showed dynamic fluctuations in the pico- to nanosecond time regime, and samples between C3'-endo and C2'-endo conformations (27, 58). Dynamics of G7 and G24 occur on micro- to millisecond timescales and they sample multiple conformations but not necessarily concerted (27, 58), and G24 flips out of the internal loop ~20% of the time. Therefore, the active site of leadzyme has both orderliness in the pre-formed metal ion binding site and dynamics for specific residues (28).

Even the crystal structures provided some clues on the flexibility of the active site (36, 37). For example, C6 adopts different sugar pucker conformations in the two different molecules Mol I and Mol II, and the different loop nucleotides have different phosphorus peak heights in their electron density maps. It was believed that the two crystal structures represent only two of an ensemble of possible solution structures that were trapped in the crystal lattice.

In the past few years, ultrafast time-resolved fluorescence spectroscopy has emerged as a new structural tool for probing RNA conformational dynamics pioneered in the Xia laboratory (70, 74). This new approach promises to provide intricate details of RNA conformational heterogeneity (30, 66, 75–79) by capturing the complex decay dynamics of a fluorophore, e.g., 2-aminopurine, incorporated in the RNA structure to deduce the ensemble of conformations and their distributions quantitatively. Typically, 2-aminopurine decay dynamics profiles due to charge transfer reaction need to be accounted for by multiple exponential components on pico- to nanosecond timescales, each representing a unique sub-family of structure with certain base stacking patterns.

Application of an ultrafast dynamics approach on leadzyme provided new insights into the complexity of the leadzyme conformational dynamics and heterogeneity (30). For base 25, at least four different states were observed, including stacking with G26 and/or G24 as observed in the NMR and crystal structures, and a sub-population that is completely unstacked, presumably similar to the conformation of this base in the MC-SYM model. Apparently, base 25 samples various states, including excursion to a conformation that resembles the catalytically active state. Ultrafast time-resolved anisotropy decay measurements showed that base 25 undergoes internal motions on multiple picosecond timescales that allow the base to sample the various structures. The bases 7, 8, and 9 on the longer strand are not well stacked within the internal loop in solution state, different from what was seen in the crystal structures (Figure 3B), and there are heterogeneous populations. Femtosecond anisotropy decay showed a main component of 140 ps internal base motion for base 8, complementing the NMR results on the sugar moiety that this base dynamically fluctuates between C3'- and C2'-endo on a sub-ns timescale (28).

The observations that 8BrG at position 24 in the active site enhanced cleavage activity (38) posed an interesting question, whether 8BrG substitution at 24 may change the distribution of conformations elsewhere in the loop such that the transition state energy barrier is lowered. By comparing the decay dynamics profiles between leadzymes with and without the 8BrG substitution at 24, it appeared that 8BrG

moderately increases the overall unstacked populations for bases 7 and 8. This is consistent with the fact that both bases need to flip out to allow the formation of C6-G9-G24 triple. Therefore, it is likely that 8BrG enhances leadzyme activity partially due to enforcing a favorable conformational distribution at these two bases in addition to favoring *syn* at G24 position.

Expert opinion and outlook

A general lesson learned from these studies on leadzyme is that RNA can sample local heterogeneity with populations typically dominated by inactive conformations that are amenable to characterization by NMR and crystallography. The NMR and crystal structures of leadzyme represent a few from an ensemble of ground states. The heterogeneity of ground state conformations is necessarily the consequence of intrinsic dynamic properties of RNA. Therefore, techniques that can reveal the full complexity of the conformational ensemble will significantly enhance our understanding of the structural basis of leadzyme catalysis.

It was obvious that leadzyme has to undergo significant conformational rearrangements to reach the catalytically active form. The transient nature of this state would escape detection by traditional structural biology tools. Modeling efforts played a significant role in providing insights on the structural features that are relevant to catalysis. It was traditional biochemical data that the model was based on, and it was smart biochemistry that helped to establish the validity of the model. Conformational changes are key events for catalysis, and the intrinsic flexibility of RNA is well suited for this task, but this poses a significant challenge for biophysicists to paint the entire pathway of conformational transition. One of the challenges would be to assess whether Pb²⁺ binding employs a conformational capture mechanism (80, 81) to promote the catalytic state. Time-resolved approaches will likely contribute to these issues.

The detailed chemistry of the Pb²⁺-induced cleavage reaction has not been fully characterized, and it was not clear whether both steps of reaction involve the same Pb²⁺ ion or not. In addition, the enhancement of reaction by rare earth ions is mysterious. One can envision that spectroscopic techniques that are sensitive to metal ions would play some role in this effort.

The research on leadzyme again demonstrated the advantage of combining different approaches. Leadzyme will continue to serve as an excellent model system for learning RNA structure, dynamics, and mechanism of catalysis.

Highlights

- Leadzyme is a small catalytic RNA selected from a library of tRNA for Pb²⁺-induced self-cleavage.
- Leadzyme exhibits strong metal ion specificity and undergoes a unique two-step cleavage mechanism. The detailed

chemistry of Pb^{2+} -induced cleavage reaction at atomic resolution has not been fully elucidated.

- Multiple structural models for leadzyme are available, including ground states and a catalytic state, but the precise mechanism of transition from ground state to the catalytically active state has not been adequately addressed.
- The dynamic nature of the active site is the key to understanding the leadzyme folding and catalysis. Various spectroscopic tools have revealed the conformational dynamics and the resulting heterogeneity of the leadzyme motif.
- Imposing conformational constraints can significantly alter the reactivity of the leadzyme. These efforts help validate the computational model of the transition state.
- Understanding the leadzyme mechanism can potentially lead to its exploration in therapy for lead toxicity.

Acknowledgments

This work was supported in part by grants from the Robert A. Welch Foundation (AT-1645) and THECB Norman Hackerman Advanced Research Program (009741-0015-2007). The authors thank Martin Fan for critical reading of the manuscript.

References

- Mendes Soares LM, Valcarcel J. The expanding transcriptome: the genome as the 'Book of Sand'. *EMBO J* 2006; 25: 923–31.
- Grosshans H, Filipowicz W. Molecular biology: the expanding world of small RNAs. *Nature* 2008; 451: 414–6.
- Elliott D, Ladomery M. Molecular biology of RNA. Oxford, UK: Oxford University Press, 2011.
- Yarus M. Life from an RNA world: the ancestor within. Cambridge, MA: Harvard University Press, 2010.
- Kruger K, Grabowski PJ, Zaug AJ, Sands J, Gottschling DE, Cech TR. Self-splicing RNA: autoexcision and autocyclization of the ribosomal RNA intervening sequence of *Tetrahymena*. *Cell* 1982; 31: 147–57.
- Guerrier-Takada C, Gardiner K, Marsh T, Pace N, Altman S. The RNA moiety of ribonuclease P is the catalytic subunit of the enzyme. *Cell* 1983; 35: 849–57.
- Gesteland RE, Cech T, Atkins JF, editors. The RNA world, 3rd ed. Woodbury, NY: Cold Spring Harbor Laboratory Press, 2006.
- Doherty EA, Doudna JA. Ribozyme structures and mechanisms. *Annu Rev Biochem* 2000; 69: 597–615.
- Lilley DMJ. Structure, folding and mechanisms of ribozymes. *Curr Opin Struct Biol* 2005; 15: 313–23.
- DeRose VJ. Two decades of RNA catalysis. *Chem Biol* 2002; 9: 961–9.
- Fedor MJ, Williamson JR. The catalytic diversity of RNAs. *Nat Rev Mol Cell Biol* 2005; 6: 399–412.
- Lilley DMJ, Eckstein F, editors. Ribozymes and RNA catalysis. RSC biomolecular sciences. Cambridge, UK: RSC Publishing, 2008.
- Toor N, Keating KS, Pyle AM. Structural insights into RNA splicing. *Curr Opin Struct Biol* 2009; 19: 260–6.
- Serganov A, Patel DJ. Ribozymes, riboswitches and beyond: regulation of gene expression without proteins. *Nat Rev Gene* 2007; 8: 776–90.
- Strobel SA, Cochrane JC. RNA catalysis: ribozymes, ribosomes, and riboswitches. *Curr Opin Chem Biol* 2007; 11: 636–43.
- Scott WG. Ribozymes. *Curr Opin Struct Biol* 2007; 17: 280–6.
- Scott WG. RNA structure, metal ions, and catalysis. *Curr Opin Chem Biol* 1999; 3: 705–9.
- David L, Lambert D, Gendron P, Major F. Leadzyme. *Methods Enzymol* 2001; 341: 518–40.
- Werner C, Krebs B, Keith G, Dirheimer G. Specific cleavages of pure tRNAs by plumbous ions. *Biochim Biophys Acta* 1976; 432: 161–75.
- Brown RS, Dewan JC, Klug A. Crystallographic and biochemical investigation of the lead(II)-catalyzed hydrolysis of yeast phenylalanine transfer-RNA. *Biochemistry* 1985; 24: 4785–801.
- Krzyzosiak WJ, Marciniak T, Wiewiorowski M, Romby P, Ebel JP, Giege R. Characterization of the lead(II)-induced cleavages in transfer-RNAs in solution and effect of the Y-base removal in yeast transfer RNA^{phe}. *Biochemistry* 1988; 27: 5771–7.
- Behlen LS, Sampson JR, Drenzo AB, Uhlenbeck OC. Lead-catalyzed cleavage of yeast transfer RNA^{phe} mutants. *Biochemistry* 1990; 29: 2515–23.
- Westhof E, Hermann T. Leadzyme RNA catalysis. *Nat Struct Biol* 1999; 6: 208–9.
- Pan T, Uhlenbeck OC. In vitro selection of RNAs that undergo autolytic cleavage with Pb^{2+} . *Biochemistry* 1992; 31: 3887–95.
- Pan T, Uhlenbeck OC. A small metalloribozyme with a 2-step mechanism. *Nature* 1992; 358: 560–3.
- Pan T, Dichtl B, Uhlenbeck OC. Properties of an in vitro selected Pb^{2+} cleavage motif. *Biochemistry* 1994; 33: 9561–5.
- Hoogstraten CG, Legault P, Pardi A. NMR solution structure of the lead-dependent ribozyme: evidence for dynamics in RNA catalysis. *J Mol Biol* 1998; 284: 337–50.
- Legault P, Hoogstraten CG, Metlitzky E, Pardi A. Order, dynamics and metal-binding in the lead-dependent ribozyme. *J Mol Biol* 1998; 284: 325–35.
- Julien KR, Sumita M, Chen PH, Laird-Offringa IA, Hoogstraten CG. Conformationally restricted nucleotides as a probe of structure-function relationships in RNA. *RNA* 2008; 14: 1632–43.
- Kadakkuzha BM, Zhao L, Xia T. Conformational distribution and ultrafast base dynamics of leadzyme. *Biochemistry* 2009; 48: 3807–9.
- Sugimoto N, Ohmichi T. Site-specific cleavage reaction catalyzed by leadzyme is enhanced by combined effect of lead and rare earth ions. *FEBS Lett* 1996; 393: 97–100.
- Ohmichi T, Sugimoto N. Role of Nd^{3+} and Pb^{2+} on the RNA cleavage reaction by a small ribozyme. *Biochemistry* 1997; 36: 3514–21.
- Chartrand P, Usman N, Cedergren R. Effect of structural modifications on the activity of the leadzyme. *Biochemistry* 1997; 36: 3145–50.
- Kim MH, Katahira M, Sugiyama T, Uesugi S. Activation and repression of the activity of a lead ribozyme by the combination of Pb^{2+} and Mg^{2+} . *J Biochem* 1997; 122: 1062–7.
- Katahira M, Kim MH, Sugiyama T, Nishimura Y, Uesugi S. Two metal-binding sites in a lead ribozyme bound to competitively by Pb^{2+} and Mg^{2+} -induced structural changes as revealed by NMR. *Eur J Biochem* 1998; 255: 727–33.
- Wedekind JE, McKay DB. Crystal structure of a lead-dependent ribozyme revealing metal binding sites relevant to catalysis. *Nat Struct Biol* 1999; 6: 261–8.
- Wedekind JE, McKay DB. Crystal structure of the leadzyme at 1.8 angstrom resolution: metal ion binding and the implications

- for catalytic mechanism and allo site ion regulation. *Biochemistry* 2003; 42: 9554–63.
38. Yajima R, Proctor DJ, Kierzek R, Kierzek E, Bevilacqua PC. A conformationally restricted guanosine analog reveals the catalytic relevance of three structures of an RNA enzyme. *Chem Biol* 2007; 14: 23–30.
 39. Barciszewska MZ, Wyszko E, Bald R, Erdmann VA, Barciszewski J. 5S rRNA is a leadzyme. A molecular basis for lead toxicity. *J Biochem* 2003; 133: 309–15.
 40. Kikovska E, Mikkelsen NE, Kirsebom LA. The naturally transacting ribozyme RNase P RNA has leadzyme properties. *Nucleic Acids Res* 2005; 33: 6920–30.
 41. Barciszewska MZ, Szymanski M, Wyszko E, Pas J, Rychlewski L, Barciszewski J. Lead toxicity through the leadzyme. *Mut Res-Rev Mut Res* 2005; 589: 103–10.
 42. Wyszko E, Nowak M, Pospieszny H, Szymanski M, Pas J, Barciszewska MZ, Barciszewski J. Leadzyme formed in vivo interferes with tobacco mosaic virus infection in *Nicotiana tabacum*. *FEBS J* 2006; 273: 5022–31.
 43. Misra VK, Shiman R, Draper DE. A thermodynamic framework for the magnesium-dependent folding of RNA. *Biopolymers* 2003; 69: 118–36.
 44. Draper DE, Grilley D, Soto AM. Ions and RNA folding. *Annu Rev Biophys Biomol Struct* 2005; 34: 221–43.
 45. Woodson SA. Metal ions and RNA folding: a highly charged topic with a dynamic future. *Curr Opin Chem Biol* 2005; 9: 104–9.
 46. Pyle AM. Ribozymes: a distinct class of metalloenzymes. *Science* 1993; 261: 709–14.
 47. Fedor MJ. The role of metal ions in RNA catalysis. *Curr Opin Struct Biol* 2002; 12: 289–95.
 48. DeRose VJ. Metal ion binding to catalytic RNA molecules. *Curr Opin Struct Biol* 2003; 13: 317–24.
 49. Doudna JA, Lorsch JR. Ribozyme catalysis: not different, just worse. *Nat Struct Mol Biol* 2005; 12: 395–402.
 50. Schnabl J, Sigel RK. Controlling ribozyme activity by metal ions. *Curr Opin Chem Biol* 2010; 14: 269–75.
 51. Kragten J. *Atlas of metal-ligand equilibria in aqueous solution*. Chichester, UK: Halsted Press, 1978.
 52. Lemieux S, Chartrand P, Cedergren R, Major F. Modeling active RNA structures using the intersection of conformational space: application to the lead-activated ribozyme. *RNA* 1998; 4: 739–49.
 53. Legault P, Pardi A. P-31 chemical-shift as a probe of structural motifs in RNA. *J Mag Res B* 1994; 103: 82–6.
 54. Legault P, Pardi A. In situ probing of adenine protonation in RNA by C-13 NMR. *J Am Chem Soc* 1994; 116: 8390–1.
 55. Mueller L, Legault P, Pardi A. Improved RNA structure determination by detection of NOE contacts to exchange-broadened amino protons. *J Am Chem Soc* 1995; 117: 11043–8.
 56. Legault P, Pardi A. Unusual dynamics and pK(a) shift at the active site of a lead-dependent ribozyme. *J Am Chem Soc* 1997; 119: 6621–8.
 57. Ohmichi T, Okumoto Y, Sugimoto N. Effect of substrate RNA sequence on the cleavage reaction by a short ribozyme. *Nucleic Acids Res* 1998; 26: 5655–61.
 58. Hoogstraten CG, Wank JR, Pardi A. Active site dynamics in the lead-dependent ribozyme. *Biochemistry* 2000; 39: 9951–8.
 59. Cai ZP, Tinoco I. Solution structure of loop a from the hairpin ribozyme from tobacco ringspot virus satellite. *Biochemistry* 1996; 35: 6026–36.
 60. Pley HW, Flaherty KM, McKay DB. Three-dimensional structure of a hammerhead ribozyme. *Nature* 1994; 372: 68–74.
 61. Scott WG, Finch JT, Klug A. The crystal-structure of an all-RNA hammerhead ribozyme – a proposed mechanism for RNA catalytic cleavage. *Cell* 1995; 81: 991–1002.
 62. Murray JB, Terwey DP, Maloney L, Karpeisky A, Usman N, Beigelman L, Scott WG. The structural basis of hammerhead ribozyme self-cleavage. *Cell* 1998; 92: 665–73.
 63. Martick M, Scott WG. Tertiary contacts distant from the active site prime a ribozyme for catalysis. *Cell* 2006; 126: 309–20.
 64. Saenger W. *Principles of nucleic acid structure*. New York: Springer-Verlag, 1984.
 65. Zimmermann GR, Shields TP, Jenison RD, Wick CL, Pardi A. A semiconserved residue inhibits complex formation by stabilizing interactions in the free state of a theophylline-binding RNA. *Biochemistry* 1998; 37: 9186–92.
 66. Lee SW, Zhao L, Pardi A, Xia TB. Ultrafast dynamics show that the theophylline and 3-methylxanthine aptamers employ a conformational capture mechanism for binding their ligands. *Biochemistry* 2010; 49: 2943–51.
 67. Uhlenbeck OC. Keeping RNA happy. *RNA* 1995; 1: 4–6.
 68. Crothers DM. RNA conformational dynamics. In: Soll D, Nishimura S, Moore PB, editors. *RNA*. Oxford: Elsevier Science Ltd., 2001: 61–70.
 69. Al-Hashimi HM, Walter, NG. RNA dynamics: it is about time. *Curr Opin Struct Biol* 2008; 18: 321–9.
 70. Xia T. Taking femtosecond snapshots of RNA conformational dynamics and complexity. *Curr Opin Chem Biol* 2008; 12: 604–11.
 71. Noeske J, Schwalbe H, Wohnert J. Metal-ion binding and metal-ion induced folding of the adenine-sensing riboswitch aptamer domain. *Nucleic Acids Res* 2007; 35: 5262–73.
 72. Lemay JF, Lafontaine DA. Core requirements of the adenine riboswitch aptamer for ligand binding. *RNA* 2007; 13: 339–50.
 73. Mulhbach J, Lafontaine DA. Ligand recognition determinants of guanine riboswitches. *Nucleic Acids Res* 2007; 35: 5568–80.
 74. Zhao L, Xia T. Probing RNA conformational dynamics and heterogeneity using femtosecond time-resolved fluorescence spectroscopy. *Methods* 2009; 49: 128–35.
 75. Xia T, Becker HC, Wan C, Frankel A, Roberts RW, Zewail AH. The RNA-protein complex: direct probing of the interfacial recognition dynamics and its correlation with biological functions. *Proc Natl Acad Sci USA* 2003; 100: 8119–23.
 76. Xia T, Wan CZ, Roberts RW, Zewail AH. RNA-protein recognition: single-residue ultrafast dynamical control of structural specificity and function. *Proc Natl Acad Sci USA* 2005; 102: 13013–8.
 77. Zhao L, Xia T. Direct revelation of multiple conformations in RNA by femtosecond dynamics. *J Am Chem Soc* 2007; 129: 4118–9.
 78. Liu JD, Zhao L, Xia T. The dynamic structural basis of differential enhancement of conformational stability by 5'- and 3'-dangling ends in RNA. *Biochemistry* 2008; 47: 5962–75.
 79. Jain N, Zhao L, Liu JD, Xia TB. Heterogeneity and dynamics of the ligand recognition mode in purine-sensing riboswitches. *Biochemistry* 2010; 49: 3703–14.
 80. Williamson JR. Induced fit in RNA-protein recognition. *Nat Struct Biol* 2000; 7: 834–7.
 81. Leulliot N, Varani G. Current topics in RNA-protein recognition: control of specificity and biological function through induced fit and conformational capture. *Biochemistry* 2001; 40: 7947–56.